Frontiers of Information Technology & Electronic Engineering
www.zju.edu.cn/jzus; engineering.cae.cn; www.springerlink.com
ISSN 2095-9184 (print); ISSN 2095-9230 (online)
E-mail: jzus@zju.edu.cn

Human hip joint center analysis for biomechanical design of a hip joint exoskeleton*

Wei YANG, Can-jun YANG†‡, Ting XU

(*State Key Laboratory of Fluid Power & Mechatronic Systems, Zhejiang University, Hangzhou 310027, China*)

†E-mail: ycj@zju.edu.cn

Received Sept. 4, 2015; Revision accepted Jan. 13, 2016; Crosschecked July 11, 2016

Abstract: We propose a new method for the customized design of hip exoskeletons based on the optimization of the human-machine physical interface to improve user comfort. The approach is based on mechanisms designed to follow the natural trajectories of the human hip as the flexion angle varies during motion. The motions of the hip joint center with variation of the flexion angle were measured and the resulting trajectory was modeled. An exoskeleton mechanism capable to follow the hip center's movement was designed to cover the full motion ranges of flexion and abduction angles, and was adopted in a lower extremity assistive exoskeleton. The resulting design can reduce human-machine interaction forces by 24.1% and 76.0% during hip flexion and abduction, respectively, leading to a more ergonomic and comfortable-to-wear exoskeleton system. The human-exoskeleton model was analyzed to further validate the decrease of the hip joint internal force during hip joint flexion or abduction by applying the resulting design.

Key words: Hip joint exoskeleton, Hip joint center, Compatible joint, Human-machine interaction force
http://dx.doi.org/10.1631/FITEE.1500286 **CLC number:** TP242.6

1 Introduction

With rapid progress in mechatronics and robotics, anthropomorphic exoskeletons have been widely studied for rehabilitation applications and for general walking assistance. Key contributions in these areas include lower extremity exoskeletons for post-stroke patient rehabilitation on treadmills (Lopes (Veneman *et al.*, 2006) and Lokomat (Hidler *et al.*, 2009)), wearable exoskeletons for paraplegic daily walking (HAL (Suzuki *et al.*, 2007), Indego (Farris *et al.*, 2011), and Rewalk (Esquenazi *et al.*, 2012)), and upper arm exoskeletons for upper body rehabilitation (Armin-III (Nef *et al.*, 2013) and IntelliArm (Ren *et al.*, 2013)). Although such exoskeletons can assist or guide the motions of humans, especially patients, there is potential for discomfort and injury if the designs are not compatible with human biomechanics (Wang *et al.*, 2014). Without the ability to fully sense discomfort, paraplegic or post-stroke patients may even suffer from serious injuries during repeated rehabilitation, where comfort is far from ideal when wearing traditional exoskeletons. To address such problems, we focus on the lower body and present a human-biomechanics-based exoskeleton for providing support to the hip joint in a natural way. Based on the human anatomical experimental data, the designed mechanical hip joint center (HJC) can follow naturally occurring motions as the flexion angle varies.

Traditional exoskeleton designs are often based on assumptions that bionic joints are simplified to 'pin and socket' or 'ball and socket' jointed engineered designs to reduce kinematic complexity. It is usually these simplifications that cause the incompatibility of the exoskeleton's motions with human movements. Schiele and van der Helm (2006) improved

‡ Corresponding author
* Project supported by the National Natural Science Foundation of China (No. 51221004)
ORCID: Can-jun YANG, http://orcid.org/0000-0002-3712-0538

ergonomics in human-machine interaction through the kinematic design of an upper-arm exoskeleton. Stienen *et al.* (2009) decoupled joint rotations and translations to make self-alignment exoskeleton axes, and the decoupling approach was applied to the upper-limb exoskeleton. Jarrasse and Morel (2012) designed kinematics of fixations between an exoskeleton and a human to improve the physical connections. Cempini *et al.* (2013) presented a complete analytical treatment of the problem of misalignment in a robotic chain for human limb torque assistance. These aforementioned approaches can effectively improve the compatibility of an upper-arm exoskeleton. However, for a lower-limb exoskeleton, a disadvantage is mainly the vertical orientation of the segments. As each exoskeleton segment is connected to each leg segment, without strong translational couplings to other exoskeleton segments, individual cuffs may slip due to gravity and cyclical inertial forces that may irritate participants (Stienen *et al.*, 2009).

Several approaches have been used to realize the alignment of the hip joint motions of a human wearing an exoskeleton. The most common approach applied is adding some form of size adjustment mechanism, e.g., HAL-3 (Kawamoto and Sankai, 2005), Lokomat (Hidler *et al.*, 2009), and ALEX (Banala *et al.*, 2009), which can help with the alignment of the hip flexion axis. However, the exoskeleton hip abduction axis cannot be regulated in this way because it leads to deviation of the hip joint between the motions of the human and the exoskeleton. Valiente (2005) designed a quasi-passive parallel leg with a cam and cam roller mechanism at the upper leg to realize hip abduction joint alignment. Because of the passive joint design, the friction caused by the mechanism results in additional energy consumption for the wearer. To address this problem, Zoss *et al.* (2006) developed the Berkeley Lower Extremity Exoskeleton (BLEEX), with its flexion and abduction rotation axes intersecting at the human HJC, which was fixed during flexion and abduction. Although these approaches have contributed to realizing better hip joint alignment, dynamic motions of HJC based on human biomechanics have not yet been accommodated for.

We present a design method without additional passive joints to improve the compatibility of the exoskeleton hip joint. The alignment of the exoskeleton hip joint to the human HJC dynamic motions is the key point of this method. To achieve this goal, the three hip joint orthogonal axes, the flexion/extension axis, the abduction/adduction axis, and the internal/external rotation axis are split and followed up with translations of the flexion/extension axis and the abduction/adduction axis. The aforementioned translations help create dynamic exoskeleton HJC motions during thigh movements to provide a full coverage of human HJC motions. Because neither additional joints nor power units are used, this method leads to a simpler exoskeleton mechanism. The method we present provides a convincing alternative for exoskeleton mechanical design aiming at joint alignment. The only challenge is that the human HJC motions need to be understood well.

Thus, an understanding and quantification of anatomical joint center motions is necessary for designing exoskeleton joints. The HJC is focused upon in this study. In a pelvic anatomical coordinate system, the motions of the HJC have been estimated previously using a functional method applied by calculating the center of the best sphere described by the trajectory of markers placed on the thigh during several trials of hip rotation (Leardini *et al.*, 1999). However, the accuracy of the functional method is affected by the hip motion range, and research shows that the shape of the hip deviates from being spherical and becomes conchoidal (Greenwald and O'Connor, 1971; Afoke *et al.*, 1984; Menschik, 1997) or aspherical (Kang, 2004). Meanwhile, results of tracking the translations of human hip joints show that the motions of the femoral head (Zakani *et al.*, 2012) indicate that the HJC is not a fixed point during thigh movements, which should be kept in mind when designing exoskeletons to support human motion. Hence, we design an experimental task including static and dynamic sections. The static section uses a functional method to calculate the static HJC and the distance between the static HJC and markers pasted on the thigh surface during a limited range of hip motions. During the dynamic section, the thigh moves freely in the reachable space and specific optimization methods based on the results from the static tests are used to calculate the dynamic motion of the HJC.

The result of the dynamic section is then used to guide the design of a more biomechanically compatible exoskeleton hip joint based on the derived mechanical HJC model. The validity of the compatible

exoskeleton hip joint is examined by studying human-machine interaction and hip joint internal forces, and the conclusions are presented.

2 Hip joint center experimental task

The experimental task of measuring HJC was designed to obtain the anatomical motions of HJC during normal walking. The OptiTrack motion capture system (Krupicka *et al*., 2014) was used in measuring walking activity. As shown in Fig. 1, seven reflective markers were pasted on the right leg. One marker was placed on the anterior superior iliac spine (ASIS) to record any shaking of the pelvis and also was regarded as the origin of the body coordinate system. Two markers were placed on the lateral femoral epicondyle (LFE) and medial femoral epicondyle (MFE) to calculate the femoral orientation based on the International Society of Biomechanics (ISB) recommendations (Wu *et al.*, 2002). Another four markers were located on the thigh surface, grouped as a block to minimize the influences of human soft tissues (Gao *et al.*, 2007). Six infrared cameras (V100: R2 (OptiTrack Inc., USA)) were placed in a semicircle pattern to record the motions of the seven markers. Three volunteers have participated in this experimental task and their details are shown in Table 1.

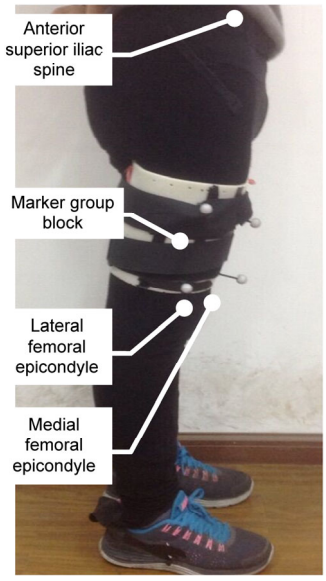

Fig. 1 Reflective marker locations

Table 1 Information of subjects for the experimental task

Subject	Gender	Age (year)	Height (cm)
1	Male	27	169
2	Male	24	170
3	Male	23	173

2.1 Static section

During static section tests, the participants were asked to lift their right leg slightly in the sagittal plane, and the flexion angle was limited within 10°. Because of the minute movements of the femoral head in the acetabulum, the HJC was assumed to stay fixed during the static section tests. Therefore, if the marker group block stays in the same position and the influence of human soft tissue is ignored, the distances between HJC and the markers in the block are invariant. This marker group block method has been shown to be a reasonable way to minimize errors introduced by human soft tissues (Gao *et al.*, 2007). Thus, the distances between the static HJC and the markers can be calculated using a functional method (Leardini *et al.*, 1999) that is well known for obtaining the optimal center of rotation position in human ball-and-socket joints. Different objective functions of the functional method were compared and validated by Camomilla *et al.* (2006). We used the Spheric-4 (S4) algorithm for its high precision and repeatability (Gamage and Lasenby, 2002).

Fig. 2 shows the implementation of the S4 algorithm with one marker on the surface of the thigh, the global coordinate system (CS), and the body CS. The global CS *O-XYZ* is defined by the motion capture system, and the body CS *o-xyz* is established

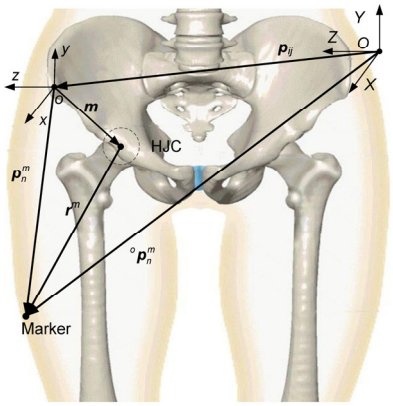

Fig. 2 Human hip coordinate systems

referring to the ISB recommendations (Wu *et al.*, 2002) with the origin *o* determined by a marker on the ASIS. Then the objective function of the S4 algorithm can be denoted by (Gamage and Lasenby, 2002)

$$f(\boldsymbol{m},\boldsymbol{r}^m)=\sum_{m=1}^{M}\sum_{n=1}^{N}\left[\|\boldsymbol{p}_n^m-\boldsymbol{m}\|^2-\|\boldsymbol{r}^m\|^2\right]^2, \quad (1)$$

where $\boldsymbol{r}^m$ and $\boldsymbol{m}$ are vectors from the HJC to the markers and the origin *o* to the HJC respectively, *M* and *N* are the marker number and sample number during thigh flexion movements respectively (we choose *M*=4 and *N*=700 in this study), and $\boldsymbol{p}_n^m$ can be calculated by

$$\boldsymbol{p}_n^m={}^o\boldsymbol{p}_n^m-\boldsymbol{p}_{ij}. \quad (2)$$

Here ${}^o\boldsymbol{p}_n^m$ denotes the position of the four markers of the block and $\boldsymbol{p}_{ij}$ denotes the position of the ASIS marker, which points from the globe CS origin *O* to the body CS origin *o*.

By minimizing Eq. (1), the HJC position can be calculated. During the static section tests, only the motions of the ASIS marker and the four markers of the block were used.

Differentiating Eq. (1) with respect to $\boldsymbol{r}^m$ and $\boldsymbol{m}$, we obtain

$$A\boldsymbol{m}=\boldsymbol{B}, \quad (3)$$

where

$$A=2\sum_{m=1}^{M}\left[\frac{1}{N}\sum_{n=1}^{N}\boldsymbol{p}_n^m\left(\boldsymbol{p}_n^m\right)^{\mathrm{T}}-\frac{1}{N}\sum_{n=1}^{N}\boldsymbol{p}_n^m\left(\frac{1}{N}\sum_{n=1}^{N}\boldsymbol{p}_n^m\right)^{\mathrm{T}}\right],$$

$$\boldsymbol{B}=\sum_{m=1}^{M}\left[\frac{1}{N}\sum_{n=1}^{N}\left(\boldsymbol{p}_n^m\right)^3-\frac{1}{N}\sum_{n=1}^{N}\left(\boldsymbol{p}_n^m\frac{1}{N}\sum_{n=1}^{N}\left(\boldsymbol{p}_n^m\right)^2\right)\right].$$

Because the optimal HJC position $\boldsymbol{m}$ is obtained, the distance between HJC and the four markers of the block can be obtained by

$$\boldsymbol{r}^m=\sqrt{\frac{1}{N}\sum_{n=1}^{N}(\boldsymbol{p}_n^m-\boldsymbol{m})},\ m=1,2,3,4. \quad (4)$$

Table 2 presents the results of six repeated experiments conducted on the first participant. The mean distance (AVE) and standard deviation (STD) of the four markers are also listed. The results show good data consistency and agree well with research results provided by Leardini *et al.* (1999).

Table 2 Distances between markers and HJC

Experiment	$\lvert\boldsymbol{r}^1\rvert$ (cm)	$\lvert\boldsymbol{r}^2\rvert$ (cm)	$\lvert\boldsymbol{r}^3\rvert$ (cm)	$\lvert\boldsymbol{r}^4\rvert$ (cm)
1	27.38	30.30	39.95	39.86
2	27.74	30.41	40.21	40.11
3	26.78	29.50	39.18	39.14
4	27.90	30.50	40.26	40.13
5	27.28	29.80	39.57	39.42
6	28.36	30.85	40.79	40.56
AVE	27.57	30.23	39.99	39.87
STD	0.55	0.49	0.56	0.52

AVE: mean distance; STD: standard deviation. $\lvert\boldsymbol{r}^1\rvert$–$\lvert\boldsymbol{r}^4\rvert$ represent the distances between markers and the HJC

2.2 Dynamic section

The participants were asked to start the dynamic section trials once they had finished the static section tests. During the dynamic section tests, the hip joints' arc movements, consisting of flexion and abduction motions, were selected because normal walking also comprises hip joint flexion and abduction motions. The participants performed the arc movements 10 times repeatedly at their self-selected speeds, and were asked to make the flexion and abduction ranges as wide as possible. Because $\boldsymbol{r}^m$ had been obtained and was considered to be constant during this section due to that the marker block was located at the same position during both sections, the optimal HJC motions of the dynamic section can be calculated by minimizing the following equation (Yan *et al.*, 2014):

$$f(\boldsymbol{m})=\sum_{m=1}^{M}\left[\|\boldsymbol{p}_n^m-\boldsymbol{m}\|^2-(\boldsymbol{r}^m)^2\right]. \quad (5)$$

During the hip joint arc movements, the flexion angle could be calculated by the two markers located on the LFE and MFE according to Eqs. (6) and (7):

$$(x_{\mathrm{FE}},y_{\mathrm{FE}},z_{\mathrm{FE}})=(\boldsymbol{v}_{\mathrm{LFE}}+\boldsymbol{v}_{\mathrm{MFE}})/2-\boldsymbol{m}, \quad (6)$$

$$\theta_{\mathrm{flex}}=\arccos\left(y_{\mathrm{FE}}\Big/\sqrt{x_{\mathrm{FE}}^2+y_{\mathrm{FE}}^2}\right), \quad (7)$$

where $\boldsymbol{v}_{\mathrm{LFE}}$ and $\boldsymbol{v}_{\mathrm{MFE}}$ are positions of markers on the LFE and MFE under body CS respectively, and θ_{flex} is

the angle of hip joint flexion during arc movements. Fig. 3 shows the spatial anatomical HJC position of participant 1 during the dynamic section.

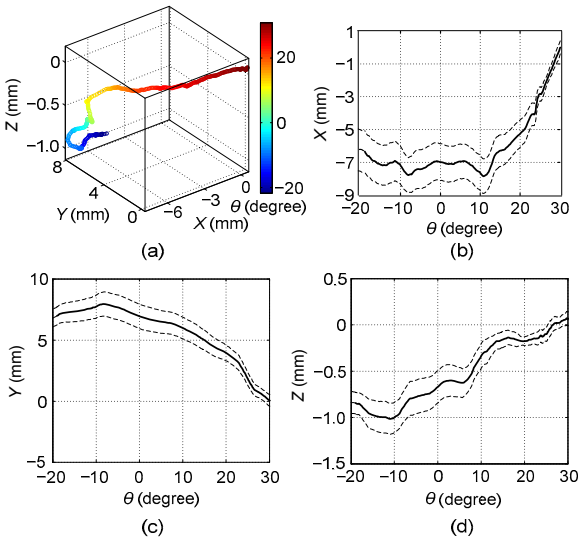

Fig. 3 HJC position during thigh arc movements
(a) HJC motion; (b) Frontal direction; (c) Lateral direction; (d) Upward direction

Considering the anatomical structure of the participants' hip joints, the HJC position should be at the same location during repeated hip joint flexion. In other words, the HJC trajectories of each trial should be curves with the same starting- and end-point. However, because of the hip joint's internal/external rotation during arc movements when adapting to flexion and abduction, it was hard for the participant to maintain a constant internal/external rotation angle and HJC trajectory between different movement trials. The results shown in Fig. 3 also confirm this. At the beginning of the arc movement, when the flexion angle is 30°, the deviations of frontal, lateral, and upward directions are quite small. When the flexion angle decreases, the deviations of all three directions increase, because the influence of the hip joint internal/external rotation angle becomes larger. The HJC's position stays almost the same while the flexion angle is within 10° in the three directions and then rises rapidly in the frontal and upward directions, and falls sharply in the lateral direction. Unlike the center of rotation movements of the knee joint (Lee and Guo, 2010) and the shoulder joint (Yan *et al.*, 2014), which are more than 30 mm, the HJC's position movement is less than 10 mm, but it is clear that it does not stay still. This result is in accordance with the findings provided by Zakani *et al.* (2012) using surgical navigation methods. Because the human-exoskeleton system is a closed chain mechanism, the misalignments of human-exoskeleton HJC positions would lead to internal forces exerted onto the participant during the closed chain mechanism's motions. Therefore, the influence of these small misalignments was analyzed and compared with the misalignment compensation design of the exoskeleton by experiments.

3 Exoskeleton hip joint design

Traditional exoskeleton hip joints were designed as ball-and-socket joints, which means that the mechanical HJC stays still during walking. Because the anatomical HJC position has been measured and found to move actually, exoskeleton hip joints should be designed to be compatible with the motions of the HJC trajectory to match with it. To keep the mechanical HJC close to the anatomical one, the sagittal, frontal, transverse, and rotation (SFTR) system was adopted, which means the joint angles in the sagittal, frontal, and transverse planes were measured. As shown in Fig. 4, a traditional three-degree-of-freedom (3-DOF) joint consisting of the *X*-, *Y*-, and *Z*-axis represents the axes of abduction/adduction, internal/external rotation, and flexion/extension, respectively. The interaction point *O* stays still when the 3-DOF joint rotates. Based on the SFTR system, a new 3-DOF joint was constructed by translations of the flexion/extension and abduction/adduction axes that were described in the *Y*-*X* and *Y*-*Z* planes respectively using polar coordinates. Both coordinates considered the *Y*-axis as the polar axis. Considering both the complexity of the mechanical design for internal/external rotation axis translation and the minor change of the internal/external rotation angle during normal gait, translation of the internal/external rotation axis was not selected. According to Fig. 4, the positions of the new intersection points, O_0 and O_1, can be expressed as follows:

$$\begin{cases} p_{O_0} = \rho_0 \mathrm{e}^{\mathrm{i}\alpha_0}, \\ p_{O_1} = \rho_1 \mathrm{e}^{\mathrm{i}\alpha_1}, \end{cases} \tag{8}$$

where ρ_0, ρ_1 and α_0, α_1 are translation distances and angles respectively, with respect to origin O and polar axis Y. Fig. 4 shows the translations of axes with which the HJC position $\boldsymbol{C}$ can be expressed as follows:

$$\begin{cases} C_x = \mathrm{Im}(A), \\ C_y = \mathrm{Re}(B), \\ C_z = \mathrm{Im}(B), \end{cases} \tag{9}$$

where

$$\begin{cases} A = \rho_1 \mathrm{e}^{-\mathrm{i}\alpha_1} + \rho_1 \mathrm{e}^{\mathrm{i}(\pi-\alpha_1-\theta_1)}, \\ B = \rho_0 \mathrm{e}^{\mathrm{i}\alpha_0} + \rho_0 \mathrm{e}^{\mathrm{i}(\alpha_0-\theta_0-\pi)} + \mathrm{Re}(A)\mathrm{e}^{-\mathrm{i}\theta_0}, \end{cases}$$

and θ_0 and θ_1 are the angles of abduction and flexion, respectively.

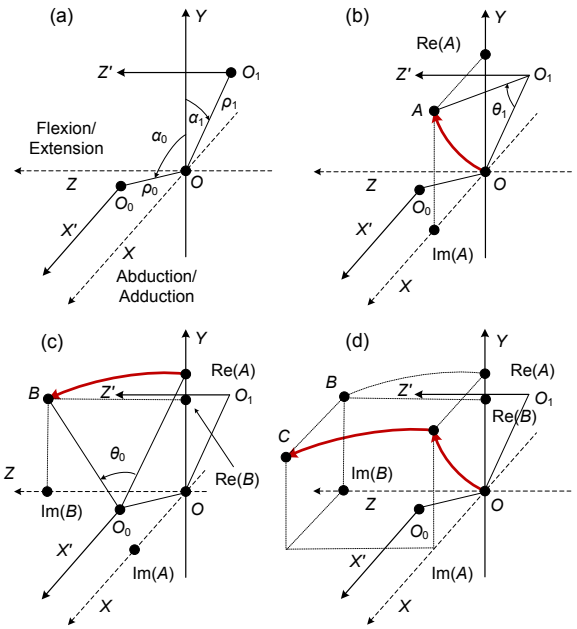

Fig. 4 Axis translations and the corresponding HJC position

(a) Translate abduction/adduction axis (X) and flexion/extension axis (Z); (b) Turning around the new flexion/extension axis (Z'); (c) Turning around the new abduction/adduction axis (X'); (d) New rotation center $\boldsymbol{C}$

With Eq. (9), the exoskeleton HJC position trajectory can be easily obtained when ρ_0, ρ_1, α_0, and α_1 are determined. The root mean square (RMS) value of the distance between the anatomical HJC and mechanical HJC was used as a criterion, with which the four design parameters could be obtained. As shown in Eq. (10), the four design parameters are considered to be optimal when $\bar{E}$ achieves its minimum value:

$$\bar{E} = \sqrt{\frac{1}{N}\sum_{i=1}^{N}\left[(O_{x_i}-C_{x_i})^2 + (O_{y_i}-C_{y_i})^2 + (O_{z_i}-C_{z_i})^2\right]}, \tag{10}$$

where $(O_{x_i}, O_{y_i}, O_{z_i})$ and $(C_{x_i}, C_{y_i}, C_{z_i})$ are the anatomical and mechanical HJC positions respectively, during the same hip joint arc movements. Applying the steepest descent method (Fletcher and Powell, 1963), the minimum value of $\bar{E}$ and the corresponding translation parameters ρ_0, ρ_1, α_0, and α_1 can be obtained. Table 3 shows the minimum values and translation parameters of these three participants.

Fig. 5 shows the optimal mechanical HJC sphere and anatomical HJC based on participant 1. The origin here denotes the human initial HJC. The anatomical HJC matches well with the mechanical HJC sphere when the flexion angle is within 0°–30°, while the deviation is enlarged when the flexion angle is within −20°–0°. However, if the mechanical HJC

Table 3 Optimal parameters for exoskeleton hip joint alignment

Subject	$\bar{E}$ (mm)	ρ_0 (mm)	ρ_1 (mm)	α_0 (°)	α_1 (°)
1	1.08	11.5	4.1	278.2	243.1
2	1.52	18.6	5.2	281.4	289.3
3	1.24	19.7	4.0	261.8	296.9

ρ_0, ρ_1, α_0, and α_1 are axis translation parameters

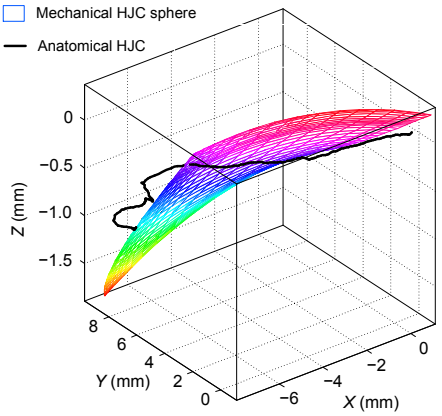

Fig. 5 Optimal mechanical HJC sphere and anatomical HJC

stays still at the origin, the deviation will be much larger. Considering the simplicity of the biocompatible joint, these results show that adopting such an approach in the design of exoskeletons could be quite beneficial in enhancing the comfort of wearers.

To realize a compatible hip joint mechanism, the optimal results were applied to translate both the abduction/adduction axis and the flexion/extension axis (Figs. 6a and 6b). The traditional exoskeleton HJC is the intersection of the abduction/adduction axis and the flexion/extension axis, which means that the HJC stays still during hip joint motions. Translation of both axes made them lie in different surfaces. Fig. 6d shows the compatible hip joint model and the traditional hip joint model as well for comparison. Applying axis translation vectors $\boldsymbol{V}_1$, $\boldsymbol{V}_2$, $\boldsymbol{V}_3$, and $\boldsymbol{V}_4$, the axis translation mechanism is acquired, which helps make both the abduction/adduction axis and the flexion/extension axis lie in the desired surfaces. In Fig. 6f, the 3D printed mechanism for axis translations makes the HJC move along the optimized mechanical HJC sphere during hip joint motions. The translation vectors $\boldsymbol{V}_1$, $\boldsymbol{V}_2$, $\boldsymbol{V}_3$, and $\boldsymbol{V}_4$ are also shown with yellow arrows for better understanding of axis translations.

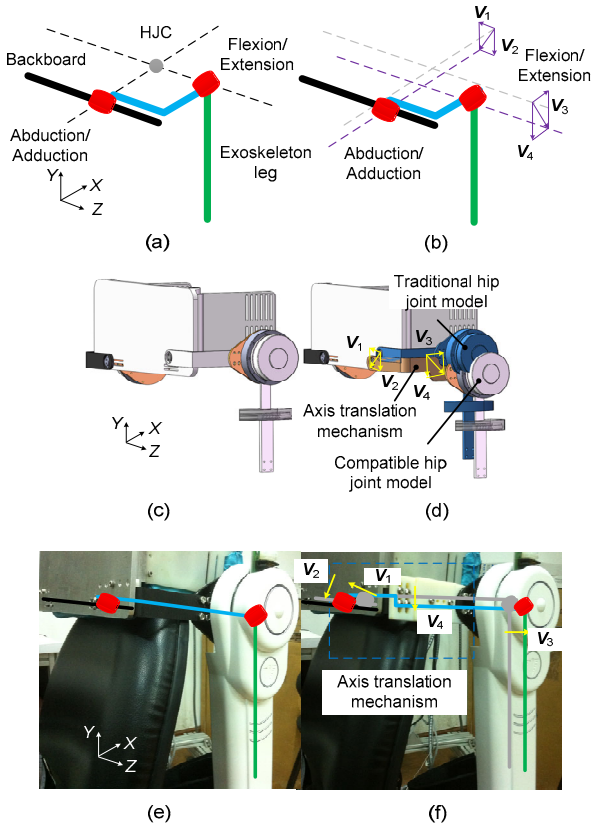

Fig. 6 Traditional and compatible hip joint mechanism design

(a) Sketch of traditional exoskeleton HJC; (b) Sketch of compatible exoskeleton HJC; (c) Traditional hip joint model; (d) Compatible hip joint model; (e) Traditional hip joint mechanism; (f) Compatible hip joint mechanism. References to color refer to the online version of this figure

The translation vectors $\boldsymbol{V}_1$, $\boldsymbol{V}_2$, $\boldsymbol{V}_3$, and $\boldsymbol{V}_4$ can be expressed as follows:

$$\boldsymbol{V}=\boldsymbol{\rho\alpha}, \tag{11}$$

where $\boldsymbol{V}=[\boldsymbol{V}_1, \boldsymbol{V}_2, \boldsymbol{V}_3, \boldsymbol{V}_4]^{\mathrm{T}}$, $\boldsymbol{\rho}=\mathrm{diag}(\rho_0, \rho_0, \rho_1, \rho_1)$, and $\boldsymbol{\alpha}=[\sin\alpha_0, \cos\alpha_0, \sin\alpha_1, \cos\alpha_1]^{\mathrm{T}}$.

Considering the diversity of the various participants' skeletal parameters, this method uses experimental data from one participant to translate the exoskeleton hip abduction/adduction axis and flexion/extension axis. This indicates that the resultant mechanism is individually suitable for the participant who provides the experimental data. However, the axis translation parameters of each participant can be acquired and calculated, and the human-exoskeleton HJC alignment can then be realized by adjustment of the aforementioned 3D printed mechanism according to the translation parameters. These three participants' HJC motions were acquired through the static and dynamic sections. Each experimental result leads to independent exoskeleton HJC axis translation parameters (Table 3).

For a correct alignment of the exoskeleton joints to human joints, the human ASIS point was selected as a reference point. Because the vector from ASIS to the human initial HJC point $\boldsymbol{m}$ had been calculated, the relative position between ASIS and exoskeleton initial HJC point was made explicit. Hence, the exoskeleton joint could be aligned to the human joint based on this relative position.

4 Experimental results and discussion

An anthropomorphic lower extremity exoskeleton with biocompatible hip joints was designed and manufactured by implementing the optimal translation parameters. The exoskeleton hip and knee flexion/extension joints were driven by flat motors

(Maxon Inc., Sachseln, Switzerland) with harmonic gearboxes (CTKM Inc., Beijing, China). Fig. 7a shows the exoskeleton structure worn by a patient. The participant's ASIS was used as the reference point for the exoskeleton hip joint to guarantee an accurate HJC alignment. The comfort of the human-exoskeleton physical interface is mostly evaluated by the interaction forces between the human and the exoskeleton (Lenzi *et al.*, 2011). This misalignment between the human and the exoskeleton HJC gives rise to an interaction force, which presses onto the human soft tissues and reduces the wearing comfort. Furthermore, the internal forces of the hip joint caused by additional human-machine forces can cause injury to the femoral head and the acetabulum. Therefore, to assess the comfort quality of the resulting exoskeleton, these physical interaction forces at the hip joint were compared with the traditional design. The interaction forces were measured by packaged force sensors consisting of two one-dimensional force sensors (Tecsis Inc., Offenbach, Germany) as shown in Fig. 7b.

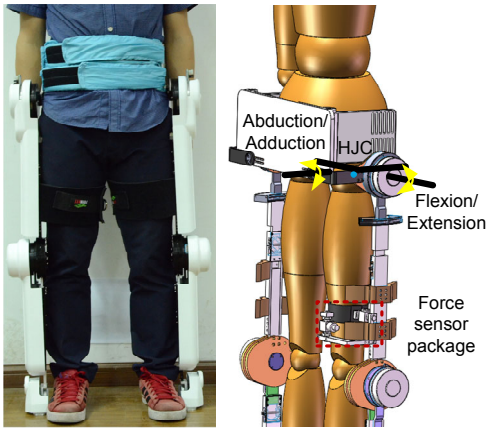

Fig. 7 Exoskeleton system
(a) Exoskeleton structure; (b) Interaction force test-bed

4.1 Human-exoskeleton interaction tests

The test volunteers were asked to participate in the interaction force experiments, which were approved by the Institutional Review Board of Zhejiang University. Informed consent was obtained from each participant. The hip flexion and abduction movements were repeated by the participant with the exoskeleton five times. The constraint conditions for the experiment were: (1) the exoskeleton hip joint flexion speed was set at 15°/s and the abduction speed was set at 10°/s; (2) the exoskeleton flexion/extension range was −20°–30° and the abduction/adduction range was 0°–30°. Fig. 8 shows the mean interaction force between participant 1 and the exoskeleton during flexion and abduction movements driven by the exoskeleton. $F_{e\theta}$ compatible and F_{er} compatible mean the normal and tangential interaction forces with respect to the connecting surface when wearing the exoskeleton with the compatible hip joint respectively, while $F_{e\theta}$ traditional and F_{er} traditional refer to the normal and tangential interaction forces with respect to the contact surface when wearing the traditional hip jointed exoskeleton respectively. Both normal and tangential forces with compatible joints decrease during flexion movements. However, only the tangential force with compatible joint decreases during abduction movements. Table 4 shows the averaged interaction force reduction during flexion and

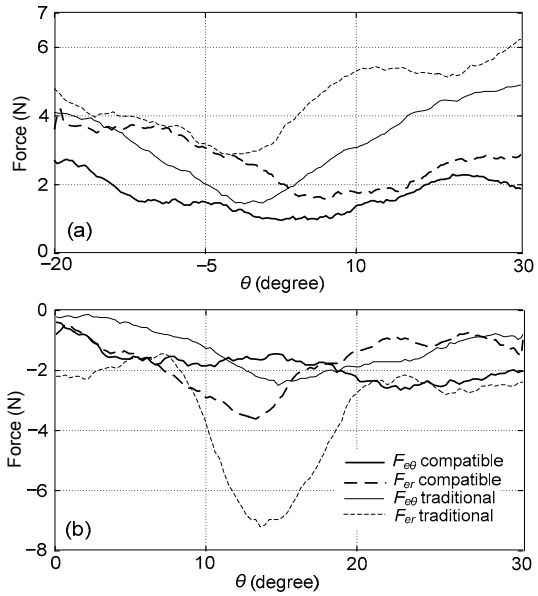

Fig. 8 Interaction force during flexion (a) and abduction (b)

Table 4 Interaction force reduction during flexion and abduction

Subject	Flexion (%)	Abduction (%)
1	25.5	85.5
2	22.1	63.1
3	24.8	79.4

abduction when the compatible hip joint design method was applied. The results show the advantage of the biocompatible hip jointed exoskeleton over the traditional one. However, the normal forces in the biocompatible jointed exoskeleton are close to the forces in the traditional joint during abduction movements. A reasonable explanation might be that the abduction speed is slow and the anatomical HJC movement in the Z direction is not significant, as shown in Fig. 3.

4.2 Effect of exoskeleton on internal hip joint force

To study further the influence of the biocompatible jointed exoskeleton on the participant, the internal hip joint force was calculated by applying kinematic and kinetic analysis of the human-exoskeleton model (Fig. 9). O_H and O_E are the HJC positions of the human and exoskeleton, respectively, which would move along the trajectories given in Fig. 9a. E is the connection point where the packaged force sensors were located.

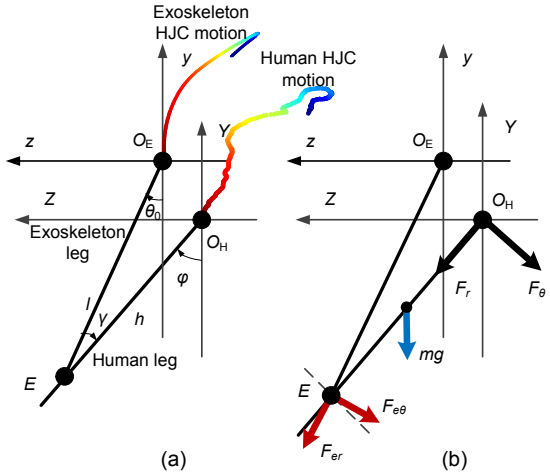

Fig. 9 Human-exoskeleton model during abduction
(a) Kinematic parameters; (b) Kinetic parameters

According to the human-exoskeleton modeling analysis, the kinematic and kinetic equations can be obtained, as listed in Eqs. (12) and (13):

$$\begin{cases} l\cdot\sin\theta_0+\Delta z=h\cdot\sin\varphi, \\ l\cdot\cos\theta_0-\Delta y=h\cdot\cos\varphi, \\ \varphi=\theta_0+\gamma, \end{cases} \tag{12}$$

$$\begin{cases} m_h(\dot{h}\dot{\varphi}+h\ddot{\varphi})=m_hg\sin\varphi+F_\theta+F_{er}\sin\gamma+F_{e\theta}\cos\gamma, \\ m_h(\ddot{h}-h\dot{\varphi}^2)=m_hg\cos\varphi+F_r+F_{er}\cos\gamma-F_{e\theta}\sin\gamma, \end{cases} \tag{13}$$

where γ is the angle deviation between the participant's abduction angle φ and the exoskeleton's abduction angle θ_0, l and h are the distances from the connection point E to O_E and O_H respectively, Δy and Δz are the distances between O_E and O_H in the Y and Z directions respectively, F_θ is the hip joint's internal force perpendicular to the thigh while F_r is parallel to the thigh, m_h is the mass of human, and g is acceleration of gravity. Fig. 10 shows the results of human-exoskeleton modeling analysis. The internal force F_r with the biocompatible joint is lower than the F_r obtained using the traditional jointed exoskeleton during flexion and abduction motions. Although the reduction of internal forces in the hip joint is not quite notable, it will relieve the loads on the femoral head and acetabulum, which would make sense in considering the repeated movements during rehabilitation with the exoskeleton. Moreover, the internal force F_θ with the biocompatible jointed exoskeleton is similar to the F_θ obtained using the traditional jointed system, which is a reasonable result considering that the applied normal interaction forces are almost the same.

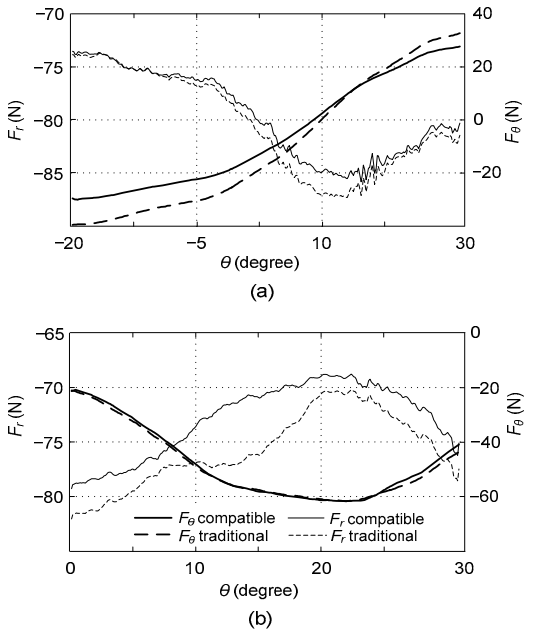

Fig. 10 Hip joint internal force during flexion (a) and abduction (b)

5 Conclusions

To realize biocompatible human-exoskeleton physical interfaces, a new method was presented and adopted to design a lower extremity exoskeleton with compatible hip joints. The compatibility of the new hip joint was validated by human-machine interaction force experiments, compared with that using an exoskeleton with traditional joints. The internal forces on the hip joint were analyzed and calculated as further evidence for the superiority of the new hip joint. The design method can also be adopted as a reference for hip replacement mechanical design and other exoskeleton compatible joint design.

The key results of this research are summarized as follows:

1. The dynamic HJC motions were calculated based on the functional method and specific optimization. The results provide evidence for that the hip joint does not constitute a simple ball-and-socket mechanism, which is in accordance with previous research reports in the area.

2. The mechanical hip joint was designed with its HJC best covering the anatomical one by translation of the flexion/extension and abduction/adduction axes under the SFTR system. The RMS error of matching is low compared with the range of anatomical HJC motions, which is about 10 mm.

3. The human-exoskeleton interaction force experiments show that the average force decreases by 24.1% and 76.0% during hip flexion and abduction, respectively, when applying the new design method. Meanwhile, the hip joint's internal force reduction validates the compatibility of the new hip joint exoskeleton. Because neither redundant joints nor complex mechanisms are added, the method presented is attractive for exoskeleton hip joint design.

In this research, each set of experimental data was acquired from one participant, because the HJC varies among different participants owing to diverse skeleton sizes. Three volunteers participated in the experiments. Therefore, participants with a wide range of anthropometric dimensions need to be examined, and the influence of different sizes on HJC motion should be studied statistically. Additionally, the adopted RMS criterion provides a global optimization that avoids large deviations. The normal-gait-data-based criteria would be a better determination for mechanical HJC, because the exoskeleton is used for walking assistance. Finally, performance evaluation at various walking speeds and various ranges of lower leg motions need to be studied further. All of these items will be studied in the next step in our research.

Acknowledgements

Many thanks to Qian-xiao WEI and Yi-bing ZHAO for assisting with the experiments, and to Prof. Gurvinder Singh VIRK and Dr. Jan VENEMAN for aiding in the writing of the paper.

References

Afoke, N.Y., Byers, P.D., Hutton, W.C., 1984. The incongruous hip joint: a loading study. *Ann. Rheum. Dis.*, **43**(2):295-301. http://dx.doi.org/10.1136/ard.43.2.295

Banala, S.K., Kim, S.H., Agrawal, S.K., *et al*., 2009. Robot assisted gait training with active leg exoskeleton (ALEX). *IEEE Trans. Neur. Syst. Rehabil. Eng.*, **17**(1):2-8. http://dx.doi.org/10.1109/tnsre.2008.2008280

Camomilla, V., Cereatti, A., Vannozzi, G., *et al.*, 2006. An optimized protocol for hip joint centre determination using the functional method. *J. Biomech.*, **39**(6):1096-1106. http://dx.doi.org/10.1016/j.jbiomech.2005.02.008

Cempini, M., de Rossi, S.M.M., Lenzi, T., *et al.*, 2013. Self-alignment mechanisms for assistive wearable robots: a kinetostatic compatibility method. *IEEE Trans. Robot.*, **29**(1):236-250. http://dx.doi.org/10.1109/TRO.2012.2226381

Esquenazi, A., Talaty, M., Packel, A., *et al.*, 2012. The ReWalk powered exoskeleton to restore ambulatory function to individuals with thoracic-level motor-complete spinal cord injury. *Am. J. Phys. Med. Rehabil.*, **91**(11):911-921. http://dx.doi.org/10.1097/PHM.0b013e318269d9a3

Farris, R.J., Quintero, H.A., Goldfarb, M., 2011. Preliminary evaluation of a powered lower limb orthosis to aid walking in paraplegic individuals. *IEEE Trans. Neur. Syst. Rehabil. Eng.*, **19**(6):652-659. http://dx.doi.org/10.1109/tnsre.2011.2163083

Fletcher, R., Powell, M.J., 1963. A rapidly convergent descent method for minimization. *Comput. J.*, **6**(2):163-168. http://dx.doi.org/10.1093/comjnl/6.2.163

Gamage, S.S.H.U., Lasenby, J., 2002. New least squares solutions for estimating the average centre of rotation and the axis of rotation. *J. Biomech.*, **35**(1):87-93. http://dx.doi.org/10.1016/S0021-9290(01)00160-9

Gao, B., Conrad, B.P., Zheng, N., 2007. Comparison of skin error reduction techniques for skeletal motion analysis. *J. Biomech.*, **40**(s2):S551. http://dx.doi.org/10.1016/S0021-9290(07)70541-9

Greenwald, A.S., O'Connor, J.J., 1971. The transmission of load through the human hip joint. *J. Biomech.*,

4(6):507-528.
http://dx.doi.org/10.1016/0021-9290(71)90041-8

Hidler, J., Nichols, D., Pelliccio, M., *et al.*, 2009. Multicenter randomized clinical trial evaluating the effectiveness of the Lokomat in subacute stroke. *Neurorehabil. Neur. Repair*., **23**(1):5-13.
http://dx.doi.org/10.1177/1545968308326632

Jarrasse, N., Morel, G., 2012. Connecting a human limb to an exoskeleton. *IEEE Trans. Robot.*, **28**(3):697-709.
http://dx.doi.org/10.1109/TRO.2011.2178151

Kang, M.J., 2004. Hip joint center location by fitting conchoid shape to the acetabular rim region of MR images. Proc. 26th Annual Int. Conf. of the IEEE. p.4477-4480.
http://dx.doi.org/10.1109/iembs.2004.1404244

Kawamoto, H., Sankai, Y., 2005. Power assist method based on phase sequence and muscle force condition for HAL. *Adv. Robot.*, **19**(7):717-734.
http://dx.doi.org/10.1163/1568553054455103

Krupicka, R., Szabo, Z., Viteckova, S., *et al*., 2014. Motion capture system for finger movement measurement in parkinson disease. *Radioengineering*, **23**(2):659-664.

Leardini, A., Cappozzo, A., Catani, F., *et al.*, 1999. Validation of a functional method for the estimation of hip joint centre location. *J. Biomech.*, **32**(1):99-103.
http://dx.doi.org/10.1016/S0021-9290(98)00148-1

Lee, K.M., Guo, J., 2010. Kinematic and dynamic analysis of an anatomically based knee joint. *J. Biomech.*, **43**(7):1231-1236.
http://dx.doi.org/10.1016/j.jbiomech.2010.02.001

Lenzi, T., Vitiello, N., de Rossi, S.M.M., *et al.*, 2011. Measuring human–robot interaction on wearable robots: a distributed approach. *Mechatronics*, **21**(6):1123-1131.
http://dx.doi.org/10.1016/j.mechatronics.2011.04.003

Menschik, F., 1997. The hip joint as a conchoid shape. *J. Biomech.*, **30**(9):971-973.
http://dx.doi.org/10.1016/S0021-9290(97)00051-1

Nef, T., Riener, R., Müri, R., *et al*., 2013. Comfort of two shoulder actuation mechanisms for arm therapy exoskeletons: a comparative study in healthy subjects. *Med. Biol. Eng. Comput*., **51**(7):781-789.
http://dx.doi.org/10.1007/s11517-013-1047-4

Ren, Y.P., Kang, S.H., Park, H.S., *et al.*, 2013. Developing a multi-joint upper limb exoskeleton robot for diagnosis, therapy, and outcome evaluation in neurorehabilitation. *IEEE Trans. Neur. Syst. Rehabil. Eng.*, **21**(3):490-499.
http://dx.doi.org/10.1109/tnsre.2012.2225073

Schiele, A., van der Helm, F.C.T., 2006. Kinematic design to improve ergonomics in human machine interaction. *IEEE Trans. Neur. Syst. Rehabil. Eng.*, **14**(4):456-469.
http://dx.doi.org/10.1109/TNSRE.2006.881565

Stienen, A.H.A., Hekman, E.E.G., van der Helm, F.C.T., *et al.*, 2009. Self-aligning exoskeleton axes through decoupling of joint rotations and translations. *IEEE Trans. Robot.*, **25**(3):628-633.
http://dx.doi.org/10.1109/TRO.2009.2019147

Suzuki, K., Mito, G., Kawamoto, H., *et al.*, 2007. Intention-based walking support for paraplegia patients with Robot Suit HAL. *Adv. Robot.*, **21**(12):1441-1469.

Valiente, A., 2005. Design of a Quasi-Passive Parallel Leg Exoskeleton to Augment Load Carrying for Walking. MS Thesis, Massachusetts Institute of Technology, Boston, USA.

Veneman, J.F., Ekkelenkamp, R., Kruidhof, R., *et al.*, 2006. A series elastic- and bowden-cable-based actuation system for use as torque actuator in exoskeleton-type robots. *Int. J. Robot. Res*., **25**(3):261-281.
http://dx.doi.org/10.1177/0278364906063829

Wang, D., Lee, K.M., Guo, J., *et al*., 2014. Adaptive knee joint exoskeleton based on biological geometries. *IEEE/ASME Trans. Mech*., **19**(4):1268-1278.
http://dx.doi.org/10.1109/TMECH.2013.2278207

Wu, G., Siegler, S., Allard, P., *et al.*, 2002. ISB recommendation on definitions of joint coordinate system of various joints for the reporting of human joint motion—part I: ankle, hip, and spine. *J. Biomech.*, **35**(4):543-548.
http://dx.doi.org/10.1016/S0021-9290(01)00222-6

Yan, H., Yang, C., Zhang, Y., *et al.*, 2014. Design and validation of a compatible 3-degrees of freedom shoulder exoskeleton with an adaptive center of rotation. *J. Mech. Des.*, **136**(7):071006.
http://dx.doi.org/10.1115/1.4027284

Zakani, S., Smith, E.J., Kunz, M., *et al.*, 2012. Tracking translations in the human hip. ASME Int. Mechanical Engineering Congress and Exposition, p.109-115.
http://dx.doi.org/10.1115/IMECE2012-87882

Zoss, A.B., Kazerooni, H., Chu, A., 2006. Biomechanical design of the Berkeley lower extremity exoskeleton (BLEEX). *IEEE/ASME Trans. Mech.*, **11**(2):128-138.
http://dx.doi.org/10.1109/TMECH.2006.871087